Locally self-similar phase diagram of the disordered Potts model on the hierarchical lattice

J-Ch. Anglès d'Auriac[1] and Ferenc Iglói[2,3,*]

[1]*Institut Néel-MCBT CNRS U.P.R. 5001 du CNRS, Laboratoire conventionné avec l'Université Joseph Fourier, B. P. 166, F-38042 Grenoble, France*

[2]*Wigner Research Centre, Institute for Solid State Physics and Optics, H-1525 Budapest, P.O. Box 49, Hungary*

[3]*Institute of Theoretical Physics, Szeged University, H-6720 Szeged, Hungary*

(Received 26 November 2012; published 4 February 2013)

We study the critical behavior of the random q-state Potts model in the large-q limit on the diamond hierarchical lattice with an effective dimensionality $d_{\rm eff} > 2$. By varying the temperature and the strength of the frustration the system has a phase transition line between the paramagnetic and the ferromagnetic phases which is controlled by four different fixed points. According to our renormalization group study the phase boundary in the vicinity of the multicritical point is self-similar; it is well represented by a logarithmic spiral. We expect an infinite number of reentrances in the thermodynamic limit; consequently one cannot define standard thermodynamic phases in this region.

DOI: 10.1103/PhysRevE.87.022103 PACS number(s): 05.50.+q, 05.10.Cc

I. INTRODUCTION

Disorder is an inevitable feature of real materials and it could result in dramatic changes in the physical properties of the systems, in particular in the vicinity of phase-transition points. The effect of disorder can be even more pronounced when both random ferromagnetic and antiferromagnetic couplings are present. Then the combined effect of frustration as well as thermal and disorder fluctuations could lead to a rich phase diagram, which contains a spin-glass (SG) phase and different critical and multicritical points [1].

Among the models studied in this context the random bond q-state Potts model [2–7] plays an important role. For $q = 2$ we have the well-known Edwards-Anderson model [8] of Ising SG and for $q = 3$ and $q = 4$ it is used to describe orientational and quadropular glasses [9], respectively. For large values of q the model is suggested to be a plausible model of supercooled liquids. This relation seems to be correct in the infinite-range model [10], but for a system with finite-range interactions further studies are needed to clarify this point. On the cubic lattice for $q = 3$ [11,12] and later for $q = 5$ and 6 [13] numerical evidence was obtained in favor of a thermodynamic transition into a stable SG phase. For $q = 10$ on the cubic lattice in the first studies no SG phase has been observed [11,12]. Repeating the calculation on a one-dimensional chain with long-range power-law interactions, which is equivalent to a short-ranged system below the upper critical dimension, evidence is obtained for an SG phase at low enough temperature [14]. Continuing this study further for even larger q-s seems to be very difficult, in particular due to the very narrow range of temperature where the presence of the SG phase is expected.

In this paper, in order to gain some insight about the possible behavior of the large-q model we use the Migdal-Kadanoff renormalization group (RG) method [15], which provides exact results on hierarchical lattices [16]. This method has already been used for the Potts model (with finite value of q) for random ferromagnetic couplings [17–20], while for random ferro- and antiferromagnetic couplings this method is combined with the Gaussian approximation [21]. Studies of the model in the large-q limit have been performed by one of the present authors in Ref. [22] to which we will refer as paper I. In paper I the lattice with an effective dimensionality, $d_{\rm eff} = 2$, is studied in more detail, in which case the critical properties of the model are calculated by solving numerically a set of integral equations.

In this paper we continue these studies when the diamond hierarchical lattice has a larger branching number, $b > 2$, which corresponds to $d_{\rm eff} > 2$. In this case the RG equations are more complicated, which are then iterated numerically. For different values of b we determine the phase diagram in the temperature-frustration plane, which is found to contain a ferromagnetic and a paramagnetic phase, but there is no SG phase. The phase transition is shown to be controlled by a random ferromagnet (RF) fixed point when the driving force of the transition is the temperature, whereas it is controlled by a zero temperature (Z) fixed point when the driving force is frustration. We calculate the critical exponents in the two attractive fixed points for different effective dimensionalities. The attractive regimes of the RF and Z fixed points in the phase transition line is separated by an unstable multicritical (MC) fixed point, the vicinity of which is studied in more detail. Our numerical investigations predict that the phase-diagram around MC has a singular structure.

The structure of the paper is the following. The model and the method of investigation is described in Sec. II. Results about the phase diagram and the critical properties of the system are presented in Sec. III, while the vicinity of the MC point is studied in Sec. IV. Our paper is closed by a Conclusion in the final section.

II. MODEL AND MIGDAL-KADANOFF RENORMALIZATION

We consider the q-state Potts model defined by the Hamiltonian:

$$\mathcal{H} = -\sum_{\langle i,j\rangle} \frac{J_{ij}}{\ln q} \delta_{s_i,s_j}, \tag{1}$$

*igloi.ferenc@wigner.mta.hu

in terms of the Potts spin variables $s_i = 1,2,\ldots,q$ at site i of the lattice. Here δ_{s_i,s_j} is the Kronecker-symbol, the summation runs over nearest-neighbor pairs and the couplings J_{ij} are independent and identically distributed random numbers, which can be either positive or negative. The $\ln q$ in the denominator insures that the transition temperature stays finite when q goes to infinity [23]. In the random cluster representation of the model the partition function $\mathcal{Z}$ is dominated by one diagram:

$$\mathcal{Z} \underset{q\to\infty}{\simeq} q^{\phi} + \text{subleading terms}, \tag{2}$$

and the free energy is given by $F = -\phi/\beta$, where $\beta = 1/T$ with the convention $k_B = 1$.

In this paper the Potts model is placed on the diamond hierarchical lattice, which is constructed recursively from a single link. At each step a link is replaced by a unit, which consists of b parallel branches, each branch containing two bonds in series. At generation n, the length L_n measured by the number of bonds between the two extreme sites A and B is $L_n = 2^n$, and the total number of bonds is

$$B_n = (2b)^n = L_n^{d_{\rm eff}(b)} \quad \text{with} \quad d_{\rm eff}(b) = \frac{\ln(2b)}{\ln 2}, \tag{3}$$

where $d_{\rm eff}(b)$ is an effective dimensionality.

In the following we consider fixed-spin boundary conditions: When the two extreme sites A and B are in the same (different) state the partition function is denoted by $\mathcal{Z}_n^{1,1}$ ($\mathcal{Z}_n^{1,2}$). Their ratio is given by

$$\frac{\mathcal{Z}_n^{1,1}}{\mathcal{Z}_n^{1,2}} = q^{I_n}, \tag{4}$$

where $I_n = \beta F_n^{\rm inter}$ and $F_n^{\rm inter} = F_n^{1,2} - F_n^{1,1}$ is the interface free energy. The scaled interface free energy I_n satisfies the recursion equation [17,19]:

$$q^{I_{n+1}} = \prod_{i=1}^{b}\left[\frac{q^{I_n^{(i_1)}+I_n^{(i_2)}} + (q-2)}{q^{I_n^{(i_1)}} + q^{I_n^{(i_2)}} + (q-2)}\right], \tag{5}$$

which for large q becomes q independent (see paper I):

$$I_{n+1} = \sum_{i=1}^{b} \Phi\left[I_n^{(i_1)}, I_n^{(i_2)}\right]. \tag{6}$$

Here the auxiliary function is

$$\Phi[I^{(1)},I^{(2)}] = \max(I^{(1)} + I^{(2)},1) - \max(I^{(1)},I^{(2)},1). \tag{7}$$

The initial condition is given by

$$I_0^{(i)} = \beta J_i, \tag{8}$$

where J_i is the value of the ith coupling.

III. PHASE DIAGRAM AND CRITICAL PROPERTIES

A. Numerical pool method

The phase diagram of the random system is studied numerically for different numbers of the branching number $b > 2$, which corresponds to an effective dimension $d_{\rm eff} > 2$. The original distribution of the couplings is given in a boxlike form:

$$\mathcal{P}(J) = \begin{cases} 1 & \text{if} \quad \frac{p}{1-p} < J < \frac{1}{1-p}, \\ 0 & \text{otherwise}, \end{cases} \tag{9}$$

with $p \leqslant 1$ as already used in paper I for $b = 2$. For $p > 0$ all couplings are random ferromagnetic and in the limit $p \to 1$ we have the pure system. For $p < 0$ there are also negative bonds; their fraction is increasing with decreasing p. In the numerical calculations we have used the so-called pool method. Since we need to perform up to 70 steps of iteration, it is not possible to proceed to a deflation of the lattice; instead we iterate a realization of the probability distribution. We start with a pool of N random variables taken from the original distribution in Eq. (9). Then we choose $2b$ numbers randomly from the pool and through renormalization at a fixed temperature T; using Eqs. (6) and (7) we generate a new parameter. Repeating this procedure N times we obtain the elements of the pool at the first generation, which are then used as input for the next renormalization step. We check the properties of the pool at each renormalization by calculating the distribution of the scaled interface free energy, its average, and its variance. In practice we have used a pool of $N = 5 \times 10^6$ elements and we went up to $n \sim$ 70–80 iterations. We mention that in order to study the sensitivity of the results on the form of the initial distribution we have also used Gaussian and symmetric bimodal distributions instead of Eq. (9), but the structure of the phase diagram and the properties of the fixed points remain the same.

B. Phases

At a given point of the phase diagram (p,T), the renormalized parameters display two different behaviors, which are governed by two trivial fixed points.

(i) In the paramagnetic phase the scaled interface free energy renormalizes to zero, thus its average is $\overline{I} = 0$ and its variance is $\Delta I = 0$.

(ii) In the ferromagnetic phase the scaled interface free energy goes to infinity. Its average behaves at a length, L as $\overline{I} \sim L^{d_s}$, with $d_s = d_{\rm eff} - 1$ being the effective dimension of the interface. Also the variance of I is divergent: $\Delta I \sim L^{\theta}$, with a droplet exponent $\theta > 0$. The length L has been defined by Eq. (3).

We note that in the large-q limit there is no spin-glass phase, even at zero temperature, contrary to the known results for $q = 2$ and $q = 3$ [24,25].

The two phases are separated by a phase transition line $T_c(p)$ which can be calculated accurately for a given pool and its true value can be obtained by averaging over different pools and taking the $N \to \infty$ limit. The phase diagrams are shown in Fig. 1 for different values of the branching number in the plane $\tau = (1+p)T/\overline{J}$ versus p. (In the vertical axis we used a nonsingular scaling combination, since the average coupling: $\overline{J} = \frac{p+1}{2}$ is zero at $p = -1$.) For the case $b \to \infty$, the exact expressions of the transition lines can be obtained and these are given in the appendix. Interestingly the phase diagram shows several reentrances in the regime $p < 0$ (see also Fig. 5). This behavior is different from that observed

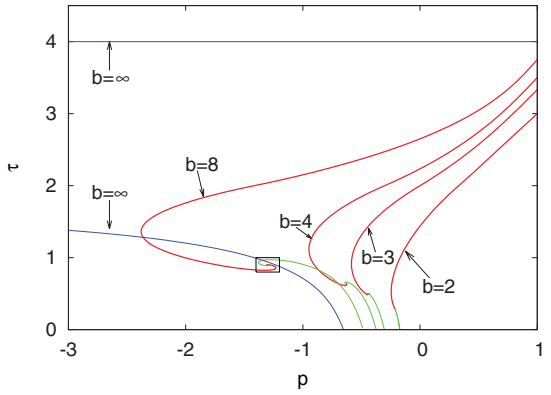

FIG. 1. (Color online) Phase diagrams for different branching numbers: $b = 2,3,4,8$, and in the $b \to \infty$ limit. The system is in the paramagnetic phase for high temperature (large T and τ) and/or for large frustration (small p); otherwise it is in the ferromagnetic phase. The phase transition lines are indicated by red (thick) and green (thin) lines, along which the transition is controlled by the RF and the Z fixed points, respectively. The red and green lines meet at the MC points where there are several reentrances for $b > 2$. For $b = 2$ the phase diagram is equivalent to that in Ref. [22].

at $b = 2$ (in which case only one reentrance is present) and we are going to study its properties in more detail in Sec. IV.

C. Fixed points

For all values of b the phase-transition line is found to be controlled by four different fixed points.

(i) The fixed point of the pure system (P) is located at $p = 1$ and $\tau = 2(2b-1)/b$ and it describes a first-order transition. This fixed point is unstable for any small amount of disorder; see paper I.

(ii) Along the transition line for $p < 1$ between P and the multicritical point MC (indicated by a red line in Fig. 1) the transition is controlled by the RF fixed point. Here $\overline{I} = \mathcal{O}(1)$ and $\Delta I = \mathcal{O}(1)$ and the distribution $P(I)$ at the fixed point is given in Fig. 2 for $b = 2,3,4$, and 8. At this fixed point the distribution contains no negative I values, but there is a δ peak at $I = 0$, the strength of which is increasing with b; see the caption of Fig. 2. In the vicinity of the transition line at a distance $\Delta T = T_c - T$ in the ferromagnetic phase the average value and the variance of I behave as

$$\overline{I}(\Delta T, L) = \left[\frac{L}{\xi_{\rm av}(\Delta T)}\right]^{d_s} + \cdots,$$
$$\Delta I(\Delta T, L) = \left[\frac{L}{\xi_{\rm var}(\Delta T)}\right]^{\theta} + \cdots. \tag{10}$$

Here the correlation lengths are divergent as $\xi_{\rm av}(\Delta T) \sim (\Delta T)^{-\nu_{\rm av}}$ and $\xi_{\rm var}(\Delta T) \sim (\Delta T)^{-\nu_{\rm var}}$, respectively.

(iii) The other part of the transition line between MC and Z (indicated by the green line in Fig. 1) is controlled by the Z fixed point, which is located at $T = \tau = 0$. Here the interface free energy grows with the size as $I(L) = L^{\theta_Z} u_I$, where the u_I are $\mathcal{O}(1)$ random numbers and the droplet exponent is $\theta_Z > 0$. Here we use the scaled variable, $i_n \equiv I_n/\overline{I}_n$, which obeys the renormalization group equation from Eq. (6):

$$\frac{I_{n+1}}{\overline{I}_n} = i_{n+1}\alpha_{n+1} = \sum_{i=1}^{b} \phi\left[i_n^{(i_1)}, i_n^{(i_2)}\right], \tag{11}$$

with $\alpha_{n+1} = \overline{I}_{n+1}/\overline{I}_n$ and

$$\phi[i^{(1)}, i^{(2)}] = \max(i^{(1)} + i^{(2)}, 0) - \max(i^{(1)}, i^{(2)}, 0). \tag{12}$$

The $T = \tau = 0$ line is an irrelevant subspace of the transformation, in which the ferromagnetic (respectively, paramagnetic) phase is located at $p > p^Z$ (respectively, $p < p^Z$) where $\alpha_n \to b$ (respectively, $\alpha_n \to 0$). In between there is the nontrivial fixed point at $p = p^Z$, in which $\alpha_n \to \alpha^Z$: α^Z is related to the droplet exponent as $\theta_Z = \log \alpha^Z / \log 2$.

The distribution of the scaled variable i is shown in Fig. 3 for various values of b. In the vicinity of the transition line at a distance $\Delta T = T_c^{'} - T^{'}$ in the ferromagnetic phase the average value and the variance of the interface free energy

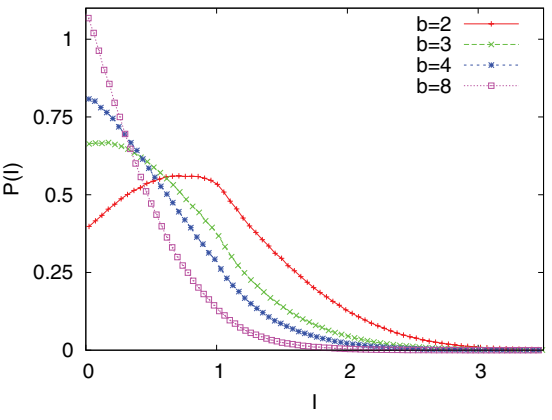

FIG. 2. (Color online) Probability distribution of the scaled interface free energy at the RF fixed point for $b = 2$, $b = 3$, $b = 4$, and $b = 8$. At $I = 0$ there is an extra δ peak with respective strength 0.12808, 0.25052, 0.31889, and 0.43609.

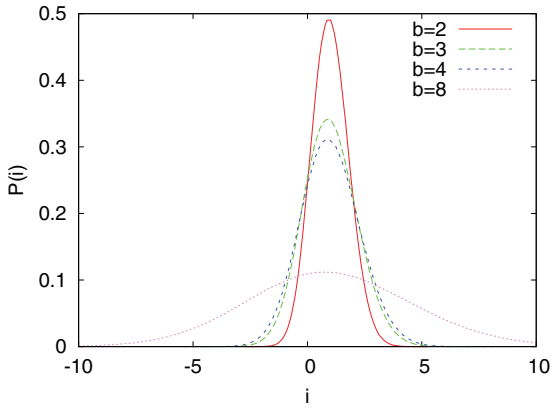

FIG. 3. (Color online) Probability distribution of the scaled interface free energy at the Z fixed point. At $i = 0$ there is a delta peak with strength $0.1728\,10^{-3}$ for $b = 2$, 0.492810^{-4} for $b = 3$, and 0.940010^{-5} for $b = 4$. For $b = 8$ and with a pool of size 5×10^6 we have found no zero value.

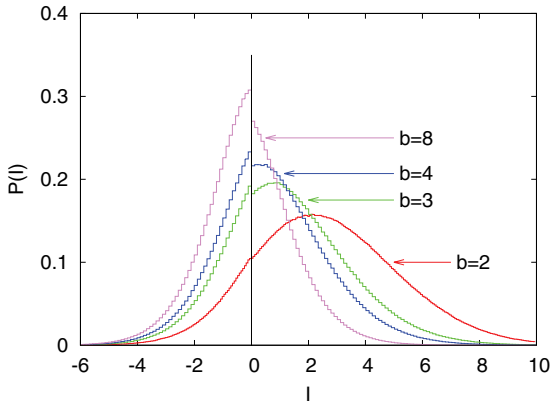

FIG. 4. (Color online) Probability distribution of the scaled interface free energy at the MC fixed point for $b = 2,3,4$, and 8. For $b > 2$ there is a discontinuity at $I = 0$ (a *step* representation of the probability distribution has been used to stress this feature). In addition there is a delta peak at $I = 0$ with respective weight 0.0057, 0.012854, 0.014713, and 0.016626 for $b = 3$, $b = 4$, and $b = 8$.

scales as

$$\overline{I}(\Delta T, L) = \frac{L^{d_s}}{[\xi_{\rm av}(\Delta T)]^{d_s-\theta_Z}} + \cdots,$$
$$\Delta I(\Delta T, L) = \frac{L^{\theta}}{[\xi_{\rm var}(\Delta T)]^{\theta-\theta_Z}} + \cdots, \quad (13)$$

respectively. Here the correlation lengths, $\xi_{\rm av}(\Delta T)$ and $\xi_{\rm var}(\Delta T)$ are divergent at $\Delta T = 0$, with the critical exponents $\nu^Z_{\rm av}$ and $\nu^Z_{\rm var}$, respectively.

(iv) The attractive regions of the RF and Z fixed points are separated by the unstable MC fixed point. Here the interface free energy behaves as $\overline{I} = \mathcal{O}(1)$ and $\Delta I = \mathcal{O}(1)$, similarly to the RF fixed point. The distribution $P(I)$ at the MC fixed point is shown in Fig. 4 for various values of b. This distribution has a finite jump at $I = 0$ for $b > 2$, which has interesting consequences about the structure of the phase diagram at MC, what we are going to analyze in Sec. IV.

D. Critical exponents

The critical exponents for $b > 2$ are calculated numerically by the pool method. In the calculation of the RF exponents we have first fixed the parameter of the disorder distribution p, then calculated the location of the critical point $T_c(p)$. For a given pool $T_c(p)$ has been calculated accurately, with a precision of 10^{-12}. Then estimates for the critical exponents are calculated from the relations in Eq. (10). At the Z fixed point the temperature is $T = 0$, therefore we have to calculate its position p_Z. Then the critical exponents are calculated from (13). Repeating the procedures for different parameters and for different pools we have obtained estimates of the set of critical exponents with a relative precision of about 10^{-3}. We have observed that the correlation length critical exponents calculated from the average and from the variance are identical for a given fixed point, i.e., $\nu_{\rm av} = \nu_{\rm var} = \nu$ and similarly $\nu^Z_{\rm av} = \nu^Z_{\rm var} = \nu^Z$. This relation is found to be exact before for $b = 2$ (see paper I) and now it is demonstrated numerically for other values of the branching number. We note that for a finite value of q the two correlation length exponents are generally different, at least on the same diamond hierarchical lattice [20]. The set of numerically calculated critical exponents are collected in Table I for different values of the branching number. For completeness we also present here the numerically exact results obtained for $b = 2$ in paper I.

TABLE I. Critical exponents of the disordered Potts model in the large-q limit on the diamond hierarchical lattice. Results for branching number $b = 2$ are from paper I.

b	2	3	4	8	16	32
θ	0.299	0.563	0.760	1.245	1.736	2.233
ν	1.307	1.051	0.949	0.808	0.730	0.684
θ_Z	0.146	0.325	0.478	0.894	1.348	1.822
ν^Z	1.729	1.258	1.051	0.738	0.555	0.440

IV. MULTICRITICAL POINT

The phase diagram in the vicinity of the MC point is different for $b = 2$ and for $b > 2$; see in Fig. 1. In the former case there is just one reentrance of the phase boundary and at the MC fixed point there is traditional multicritical behavior (see in paper I). On the contrary for $b > 2$ the phase diagram around MC has more than one reentrance. We have explored the phase diagram around MC by using larger and larger magnifications and the results for $b = 8$ are presented in Fig. 5. Interestingly the phase diagram shows a self-similar structure: The reentrances are repeated in different scales. Let us denote the location of the MC point by τ^* and p^* and then use relative positions of the phase boundary, which are given by $\Delta p = p_c - p^*$ and $\Delta\tau = \tau_c - \tau^*$. According to the results in Fig. 5 by enlarging the scale by roughly a factor of 10 the phase diagram has approximately the same reentrant structure. With the pool method, having a large, but finite number of realizations we could go up to a magnification of $\rho_0 \approx 2 \times 10^{-7}$ in the phase diagram, up to which scale one could observe at least seven similar reentrant structures.

It is instructive to use polar coordinates, ρ and ϕ, and plot the phase diagram in a semilogarithmic scale as a function of $\ln(\rho/\rho_0)$ and ϕ, which is presented in Fig. 6. In this figure the paramagnetic and the ferromagnetic phases are represented by two almost-perfect spirals, which means that the phase boundary around the MC point is approximately given by a logarithmic spiral. We note that for other values of the branching number ($b = 3$ and $b = 4$) we have observed a similar structure of the phase diagram around the MC point.

We expect that the size of the elementary magnification step ρ_0 is decreasing when the size of the pool is increasing and in the thermodynamic limit the magnification step goes to zero. In this case the phase diagram at the MC point becomes singular. Passing through the MC point the phase diagram has an infinite number of reentrances and sufficiently close to MC one cannot define a stable thermodynamic phase, since its stability range measured

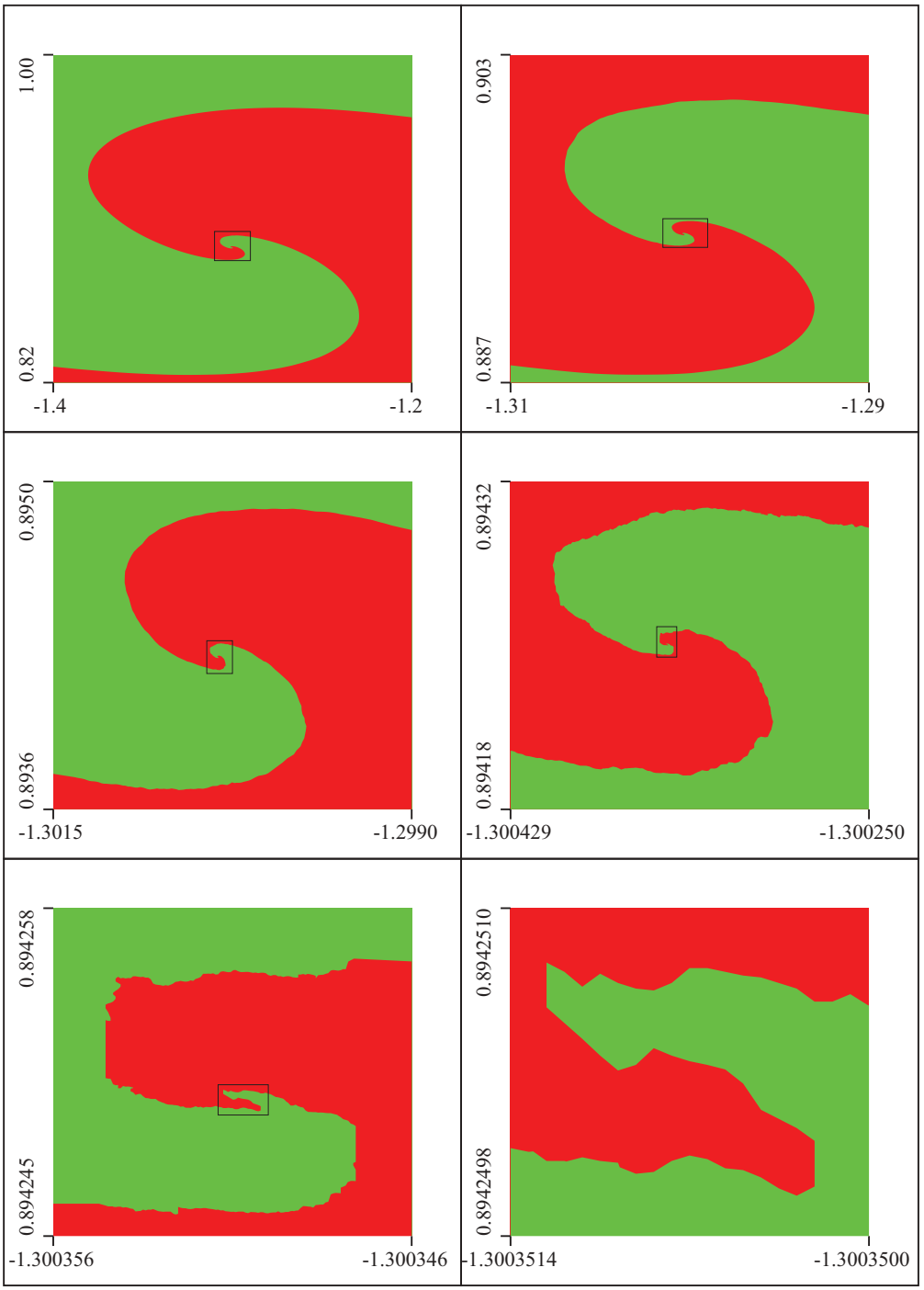

FIG. 5. (Color online) Phase diagram in the vicinity of the MP point: The framed regions are enlarged in the next figure. Note the (self-) similarity of the phase boundary in different scales. The green (bright) region represents the paramagnetic phase; the red (dark) region is the ferromagnetic phase.

either in temperature or in concentration of couplings goes to zero.

V. CONCLUSION

In this paper we considered the q-state Potts model for large q with randomly mixed ferro- and antiferromagnetic couplings and studied its critical properties on the diamond hierarchical lattice with an effective dimensionality, $d_{\text{eff}} > 2$. By using the Migdal-Kadanoff renormalization scheme, which is exact for this lattice, the phase diagram is explored numerically using the pool method. As for $d_{\text{eff}} = 2$ the phase diagram contains a ferromagnetic and a paramagnetic phase, but there is no spin-glass phase, even at zero temperature. The phase transition in the random system is controlled either by a random ferromagnet fixed point, in which the driving force is the temperature, or by a zero temperature fixed point, in which the transition is due to frustration. The two regimes are

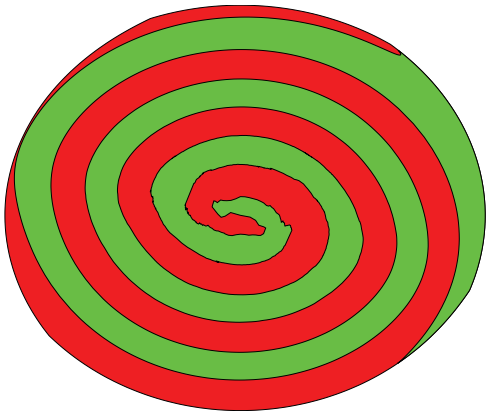

FIG. 6. (Color online) Phase diagram in the vicinity of the MP point in logarithmic polar coordinates (see text).

separated by a multicritical point in the vicinity of which the system shows unusual properties.

Both in the RF and the Z fixed points the transition is continuous and we have calculated numerically the critical exponents, which are collected in Table I. The correlation length exponents calculated from the scaling of the average or the variance are found to be equal. At the MC point the distribution of the reduced interface free energy is a discontinuous function, having a finite jump at $I = 0$. At the same time the phase diagram close to MC has a self-similar, logarithmic spiral-like structure. Consequently the phase boundary itself has a singularity and in the traditional sense one cannot define a stable thermodynamic phase here. The presence of infinitely many phase transitions at the MC point is somewhat analogous to the low-temperature phase structure of the three-dimensional axial next-nearest neighbor Ising (ANNNI) model, in which case infinitely many commensurate phases are present in the vicinity of the zero-temperature multicritical point [27]. Here one might ask the question, if the self-similar structure of the phase diagram at the MC point is related to the hierarchical nature of the lattice. Indeed, for the *nonrandom* Potts model the distribution of the zeros of the partition function on the same lattice are known to have also a fractal (self-similar) structure for finite values of q [28].

The studies presented in this paper can be extended in different directions. First, it would be interesting to study by analytical methods the behavior of the system in the vicinity of the MC point for $b > 2$. (i) To prove or disprove that the elementary magnification step at the MC point ρ_0 approaches zero in the thermodynamic limit. (ii) To show rigorously that the distribution function, $P(I)$, in the MC point is strictly discontinuous, as shown in Fig. 4. (iii) Also would be interesting to clarify the possible relation between these two expected properties.

Another extension of the present study is to investigate, if the singular behavior at the MC point could exist in another systems, too. As far as the random Potts model on hypercubic lattices is concerned it has the same fixed point structure for a finite value of q, thus generally there is an MC point in these models [24,26]. Probably in sufficiently large dimension ($d = 3$ could be enough), and for large q, the MC singularity could exist. Numerically, however, it would be very difficult to explore the details of the process, as already seen in the problem of detection of the SG phase [13,14]. A discontinuous distribution of some observables at this point, such as the reduced interface free energy, could be the sign of such singularity.

ACKNOWLEDGMENTS

The authors thank each other's institutes for facilitating visits. F.I. thanks C. Monthus and L. Turban for collaboration in related problems. He is grateful to A. N. Berker for useful discussions and to M. A. Moore for a helpful correspondence. This work has been supported by the Hungarian National Research Fund under Grants No. OTKA K75324 and No. K77629.

APPENDIX: THE PHASE DIAGRAM FOR $b \to \infty$

The phase diagram for $b \to \infty$ can be analytically treated; here we consider the initial distribution in Eq. (9). First we note that in this limit in the recursion equation [Eq. (6)] there is a sum of a large number of random variables and the renormalized value of the interface free energy depends on the sign of the average value of the auxiliary function: $\langle \Phi(I_0^{(1)}, I_0^{(2)}) \rangle \equiv \langle \Phi \rangle$. Here we can differentiate between three cases.

(i) If $\langle \Phi \rangle > 0$ then all the renormalized parameters are $I_1 \gg 1$; consequently we are at the F fixed point and due to the central limit theorem the droplet exponent is $\theta = d_s/2$.

(ii) If $\langle \Phi \rangle = 0$, then all the I_1 values are equal to zero, thus the P fixed point has been reached.

(iii) Finally, if $\langle \Phi \rangle < 0$, then all the renormalized parameters are $I_1 \ll 0$, thus in the next renormalization step we have $I_2 = 0$ and again the P fixed point has been reached.

In the next step we compute the sign of $\langle \Phi \rangle$ in the different parts of the phase diagram in Fig. 1. Let us denote the end points of the box distribution in Eq. (9) by $x = \frac{2p}{\tau}$ and $y = \frac{2}{\tau}$. In the region $y < 1$ one has $\langle \Phi \rangle = 0$ and only for $x < 0$ and $y > 1$ we can have $\langle \Phi \rangle < 0$. A direct calculation gives in this region $\langle \Phi \rangle$ as the ratio of a third degree polynomial in x and y by $(y - x)^2$ and the numerator has two different expressions according to the sign of $(x + y + 1)$. Then expressing x and y with p and τ, one gets the transition lines shown in Fig. 1. The upper boundary is a horizontal line with $\tau = 4$. The lower boundary is given by two expressions:

$$-3\tau^3 + 12\tau^2 - 24\tau + 32 + 12p\tau^2 - 48p\tau + 48p = 0$$
$$-16p^3 - 48p^2 + 24p^2\tau - \tau^3 + 16 = 0,$$

which are valid for $p < \tilde{p}$ and $p > \tilde{p}$, respectively. The two lines join at

$$\tilde{p} = \frac{1}{3}(1 - 4\cos\theta), \quad \tilde{\tau} = \frac{8}{3}(1 - \cos\theta),$$
$$\theta = \frac{\arctan(3\sqrt{7}) - \pi}{3},$$

and the extremities of the lower boundary line are at $p = -\infty$, $\tau = 2$, and $p = 2\cos(\frac{4}{9}\pi) - 1$, $\tau = 0$.

We note that in the limit $b \to \infty$ the ferromagnetic phase between $2 < \tau < 4$ extends to all values of p. For a large, but finite value of b, however, there is a paramagnetic phase for $p \lesssim -\sqrt{b}$.

[1] For reviews on spin glasses, see K. Binder and A. P. Young, Rev. Mod. Phys. **58**, 801 (1986); M. Mezard, G. Parisi, and M. A. Virasoro, *Spin Glass Theory and Beyond* (World Scientific, Singapore, 1987); K. H. Fisher and J. A. Hertz, *Spin Glasses* (Cambridge University Press, Cambridge, 1991); *Spin Glasses and Random Fields*, edited by A. P. Young (World Scientific, Singapore, 1998).
[2] D. Elderfield and D. Sherrington, J. Phys. C **16**, L497 (1983).
[3] D. J. Gross, I. Kanter, and H. Sompolinsky, Phys. Rev. Lett. **55**, 304 (1985).
[4] H.-O. Carmesin and K. Binder, J. Phys. A **21**, 4053 (1988).
[5] M. Scheucher, J. D. Reger, K. Binder, and A. P. Young, Phys. Rev. B **42**, 6881 (1990).
[6] G. Schreider and J. D. Reger, J. Phys. A **28**, 317 (1995).
[7] O. Dillmann, W. Janke, and K. Binder, J. Stat. Phys. **92**, 57 (1998).
[8] S. F. Edwards and P. W. Anderson, J. Phys. F **5**, 965 (1975).
[9] K. Binder and J. D. Reger, Adv. Phys. **41**, 547 (1992).
[10] G. Parisi, in *Complex Behavior of Glassy Systems*, edited by M. Rubi and C. Perez-Vicente (Springer, Berlin, 1997), p. 111; S. Franz and G. Parisi, Physica A **261**, 317 (1998); M. Mézard and G. Parisi, Phys. Rev. Lett. **82**, 747 (1999); M. Mézard, Physica A **265**, 352 (1999); G. Parisi, *ibid.* **280**, 115 (2000); X. Xia and P. G. Wolynes, Phys. Rev. Lett. **86**, 5526 (2001).
[11] C. Brangian, W. Kob, and K. Binder, J. Phys. A **36**, 10847 (2003).
[12] L. W. Lee, H. G. Katzgraber, and A. P. Young, Phys. Rev. B **74**, 104416 (2006).
[13] R. A. Banos *et al.*, J. Stat. Mech. (2010) P05002.
[14] R. S. Andrist, D. Larson, and H. G. Katzgraber, Phys. Rev. E **83**, 030106(R) (2011).
[15] A. A. Migdal, Sov. Phys. JETP **42**, 743 (1976); L. P. Kadanoff, Ann. Phys. (NY) **100**, 359 (1976).
[16] A. N. Berker and S. Ostlund, J. Phys. C **12**, 4961 (1979); M. Kaufman and R. B. Griffiths, Phys. Rev. B **24**, 496 (1981); R. B. Griffiths and M. Kaufman, *ibid.* **26**, 5022 (1982).
[17] W. Kinzel and E. Domany, Phys. Rev. B **23**, 3421 (1981).
[18] B. Derrida and E. Gardner, J. Phys. A **17**, 3223 (1984); B. Derrida, in *Critical Phenomena, Random Systems, Gauge Theories*, edited by K. Osterwalder and R. Stora, Proceedings of the Les Houches Summer School of Theoretical Physics, 1984 (North- Holland, Amsterdam, 1986), p. 989.
[19] D. Andelman and A. N. Berker, Phys. Rev. B **29**, 2630 (1984).
[20] C. Monthus and T. Garel, Phys. Rev. B **77**, 134416 (2008).
[21] A. Benyoussef and M. Loulidi, Phys. Rev. B **53**, 8215 (1996).
[22] F. Iglói and L. Turban, Phys. Rev. B **80**, 134201 (2009).
[23] J.-Ch. Anglès d'Auriac and F. Iglói, Phys. Rev. Lett. **90**, 190601 (2003); M.-T. Mercaldo, J.-Ch. Anglès d'Auriac, and F. Iglói, Phys. Rev. E **73**, 026126 (2006).
[24] E. S. Sorensen, M. J. P. Gingras, and D. A. Huse, Europhys. Lett. **44**, 504 (1998).
[25] I. Morgenstern and K. Binder, Phys. Rev. B **22**, 288 (1980); I. Morgenstern and H. Horner, *ibid.* **25**, 504 (1982); W. L. McMillan, *ibid.* **28**, 5216 (1983).
[26] J. L. Jacobsen and M. Picco, Phys. Rev. E **65**, 026113 (2002).
[27] For a review see W. Selke, Phys. Rep. **170**, 213 (1988).
[28] B. Derrida, L. De Seze, and C. Itzykson, J. Stat. Phys. **33**, 559 (1983).